Applied Catalysis B: Environmental 325 (2023) 122326

Contents lists available at ScienceDirect

Applied Catalysis B: Environmental

journal homepage: www.elsevier.com/locate/apcatb

Applicability and antibacterial activity of polycyclic aromatic compound derivatives used as photocatalysts for water oxidation

Yuichi Ichihashi [a,b,c,*], Tomoya Sekiguchi [a], Koki Hiramatsu [a], Yuya Tokui [a], Kazuo Kumagai [a,b], Hideto Matsuyama [a,b], Keita Taniya [a,b,c], Satoru Nishiyama [a,c]

[a] Department of Chemical Science and Engineering, Graduate School of Engineering, Kobe University, Rokkodai, Nada, Kobe 657-8501, Japan
[b] Research Center for Membrane and Film Technology, Kobe University, Rokkodai, Nada, Kobe 657-8501, Japan
[c] Social Implementation of Renewable Energy research Center, Graduate School of Engineering, Kobe University, Rokkodai, Nada, Kobe 657-8501, Japan

ARTICLE INFO

Keywords:
Photocatalytic hydrogen peroxide production
Photocatalytic antibacterial effect
Polycyclic aromatic compound derivative
Organic semiconductor

ABSTRACT

Water is oxidized using 5,8-dicyano[5]phenacene, a thin-film catalyst supported on a silica plate by vacuum deposition; hydrogen peroxide is produced under visible-light irradiation. Despite the high hydrogen peroxide production rate during the initial reaction stage, the rate decreases after 12 h, and the reaction is almost terminated after 24 h, possibly because hydrogen peroxide undergoes self-decomposition. The self-decomposition rate of hydrogen peroxide increases with increasing concentration, and attains equilibrium. Additionally, *Escherichia coli* is efficiently sterilized using this catalyst under visible-light; the antibacterial effect is exhibited even under indoor light. Among several polycyclic aromatic derivatives, 9,10-dicyanoanthracene exhibits the highest hydrogen peroxide production rate and antibacterial activity against *E. coli*. Its antibacterial efficiency is approximately 16 times higher than that of 5,8-dicyano[5]phenacene. The oxygen species causing these antibacterial effects is investigated using trapping reagents. superoxide anion radicals and hydroxyl radicals induce antibacterial effects; hydroxyl radicals are particularly effective.

1. Introduction

Titanium oxide is an oxide semiconductor; when it absorbs light energy equal to or greater than its bandgap, electrons in the valence band are excited to the conduction band to generate electron–hole pairs. Electrons and holes are known to diffuse to the surface and result in oxidation and reduction reactions with the adsorbed substances on the surface [1–9]. However, the oxidizing power is particularly strong because the redox potential is higher than that of oxidizing agents such as ozone. Under the low levels of ultraviolet (UV) light found in sources such as sunlight and indoor light in living spaces, titanium oxide photocatalysts can utilize its strong oxidizing power to decompose odors and destroy bacteria that may negatively affect everyday life. Titanium oxide thin-films are supported on glass and tiles; their deodorant, antifouling, and antibacterial effects have been evaluated under UV light irradiation in living spaces, and their excellent performance has been confirmed [5–9]. However, sunlight contains considerably lower levels of UV light than visible-light. Hence, instead of titanium oxide, a photocatalyst capable of absorbing visible-light is desirable [10,11].

Organic semiconductors have been researched and developed as excellent electronic devices [12–14]. Particularly in the field of electronics, organic semiconductors are used in devices such as solar cells, light-emitting diodes, and transistors, in addition to their application in various other fields. In recent years, organic semiconductors have attracted attention as photocatalysts [2,15–18]. The highest occupied molecular orbital (HOMO) and lowest unoccupied molecular orbital (LUMO) of organic semiconductor photocatalysts correspond to the upper end of the valence band and lower end of the conduction band of inorganic semiconductors, respectively. When an organic semiconductor is used as the photocatalyst, its HOMO and LUMO energy levels, which correspond to the oxidation potential and reduction potential, respectively, are crucial for the photocatalytic reaction.

Abbreviations: UV light, ultraviolet light; HOMO, highest occupied molecular orbital; LUMO, lowest unoccupied molecular orbital; DFT, density functional theory; E. coli., Escherichia coli; ^{1}H NMR, proton nuclear magnetic resonance spectroscopy; FT-IR, Fourier-transform infrared spectroscopy; CNPSP, 5,8-dicyano[5]phenacene thin-film on silica plate; TEMPOL, 4-hydroxy-2,2,6,6-tetramethylpiperidine-1-oxyl; IPA, 2-propanol; DMPO, 5,5-dimethyl-1-pyrroline N-oxide.

* Corresponding author at: Department of Chemical Science and Engineering, Graduate School of Engineering, Kobe University, Rokkodai, Nada, Kobe 657-8501, Japan.
E-mail address: ichiy@kobe-u.ac.jp (Y. Ichihashi).

https://doi.org/10.1016/j.apcatb.2022.122326
Received 28 October 2022; Received in revised form 20 December 2022; Accepted 24 December 2022
Available online 26 December 2022

Moreover, the wavelength of light required for the reaction depends on the HOMO–LUMO energy gap, which must be less than 3.1 eV owing to the visible-light utilization. In organic semiconductors, the HOMO and LUMO energy levels depend on the molecular structure. These energy levels can be controlled by introducing substituents into the organic semiconductors. Because the energy levels can be predicted by quantum chemical simulations using DFT calculations, the HOMO and LUMO energy levels of the photocatalysts can be easily controlled. Therefore, new photocatalysts can be developed by comprehensively considering organic semiconductors and DFT calculations. Organic semiconductors can be formed into thin-films by methods such as vacuum deposition, sputtering, and spray coating, and can also be supported by chemical bonding, thus making them convenient for various applications.

Previously, 5,8-dicyano[5]phenacene, which is a polycyclic aromatic compound organic semiconductor with a cyano group introduced into [5]phenacene, absorbed visible-light in a reducing atmosphere to decompose water and produce hydrogen [18]. Based on the HOMO–LUMO energy levels obtained from DFT calculations, we speculated that water would be oxidized in an oxygen atmosphere to produce hydrogen peroxide under the influence of 5,8-dicyano[5]phenacene. In the reaction to produce hydrogen peroxide by oxidizing water using a photocatalyst, the formation of superoxide anion radicals and hydroxyl radicals as reaction intermediates is highly possible; antibacterial effects can be expected owing to the photocatalytic effect. In this study, we investigated whether hydrogen peroxide could be produced by oxidizing water under an oxygen atmosphere over a 5,8-dicyano[5]phenacene photocatalyst, and its antibacterial activity was evaluated. In addition, the results of DFT calculations revealed that the reaction could proceed with other polycyclic aromatic compound derivatives; the hydrogen peroxide production reaction and its antibacterial effect were similarly investigated. The antibacterial efficiency was found to increase as the amount of hydrogen peroxide produced increased, and the reasons for this increase were examined. In particular, 9,10-dicyanoanthracene facilitated hydrogen peroxide generation, while demonstrating excellent antibacterial properties. When investigating the antibacterial efficiency, we observed that rather than hydrogen peroxide, the oxygen species that were formed during the hydrogen peroxide formation were responsible for the antibacterial performance. Therefore, the 9,10-dicyanoanthracene photocatalyst was comprehensively investigated, and the oxygen species responsible for its antibacterial effect were examined.

2. Experimental

2.1. Chemicals and materials

1-Naphthaldehyde (>95.0 %), 1-naphthaleneacetic acid (>98.0 %), 9,10-dicyanoanthracene (>98.0 %), 9-cyanoanthracene, 9-nitroanthracene (>95.0 %) and 2,7-dibromo-pyrene (>98.0 %) were purchased from Tokyo Chemical Industry (Tokyo, Japan). Triethylamine, acetic anhydride, methanol, toluene, sulfuric acid, iodine, benzene, magnesium sulfate, tetrahydrofuran, sodium hydroxide, and hydrochloric acid were purchased from Nacalai Tesque (Kyoto, Japan). All the reagents were of analytical grade and were used without further purification. Deionized water and acetone were used in the experiments. Titanium dioxide powder was supplied as a standard reference catalyst by the Catalysis Society of Japan (JRC-TIO-10: anatase type).

2.1.1. Catalyst preparation of 5,8-dicyano[5]phenacene

A previously reported method was used to synthesize 5,8-dicyano[5]phenacene [18]. ^{1}H NMR and FT-IR measurements confirmed that 5,8-dicyano[5]phenacene was synthesized (Figs. S1 and S2). Using the same procedure as that previously reported [18], a 5,8-dicyano[5]phenacene thin-film was deposited on a silica plate (length = 40 mm, width = 10 mm, and height = 0.5 mm) via vacuum deposition. A thickness of 300 nm was used for the deposited film. Hereafter, the prepared thin-film photocatalyst is referred to as CNPSP300.

2.1.2. Catalyst preparation of [5]phenacene-13-carboxylic acid

The following procedure was used to synthesize [5]phenacene-13-carboxylic acid [19]. Initially, 1-naphthaldehyde (0.1 mol) and 1-naphthaleneacetic acid (0.1 mol) were added to a mixture of triethylamine (10 mL) and acetic anhydride (20 mL), which was refluxed with stirring for 15 h. Ion-exchanged water (200 mL) was added to the resulting solution, which was then washed twice with ethyl acetate (250 mL), and the oil phase was collected. The recovered oil phase was washed with ion-exchanged water. Magnesium sulfate was added to remove the water. The material was filtered and then dried using an evaporator to obtain a solid, which was washed with 200 mL of ethyl acetate:heptane = 1:9 mixture to obtain a solid powder. This solid powder was recrystallized from ethyl acetate to obtain 2,3-di(naphthalen-1-yl)acrylic acid. Subsequently, the resulting 2,3-di(naphthalen-1-yl)acrylic acid (3.89 g) was added to toluene (40 mL); methanol (60 mL of) and sulfuric acid (0.640 mL) were added and refluxed under stirring for 10 h. The resulting solution was evaporated to dryness using an evaporator and also dried at 25 °C under vacuum to obtain a solid. The solid was extracted with ethyl acetate (100 mL); the oil phase was washed with ion-exchanged water, sodium bicarbonate solution, and again with ion-exchanged water. Magnesium sulfate was added to the recovered oil phase to remove water, filtered, and evaporated to dryness using an evaporator to obtain a pale-yellow solid. The solid was washed with hexane (20 mL) to obtain methyl 2,3-di(naphthalen-1-yl)acrylate. Subsequently, the resulting methyl 2,3-di(naphthalen-1-yl)acrylate (1.01 g) and iodine (0.761 g) were added to benzene (25 mL) and mixed. The solution was stirred for 12 h under UV irradiation. The resulting solution was washed with sodium sulfite and ion-exchanged water, and the oil phase was recovered. Magnesium sulfate was added to the recovered oil phase to remove the water, filtered, and evaporated to dryness using an evaporator to obtain a white solid. The solid was washed with cyclohexane (5 mL) to yield methyl [5]phenacene 13-carboxylate. Thereafter, methyl-[5]phenacene-13-carboxylate (0.336 g), ion-exchanged water (2 mL), and sodium hydroxide (0.040 g) were added to tetrahydrofuran (8 mL). The mixture was refluxed with stirring for 8 h. Hydrochloric acid was added to the resulting solution to make it acidic; ethyl acetate (50 mL) was added to the solution, which was subsequently washed with ion-exchanged water. Magnesium sulfate was added to the recovered oil phase to remove the water, filtered, and evaporated to dryness using an evaporator to obtain a solid, which was washed with cyclohexane (5 mL) to obtain the target substance, [5]phenacene-13-carboxylic acid. ^{1}H NMR and FT-IR measurements confirmed the synthesis of [5]phenacene-13-carboxylic acid (Figs. S3 and S4).

2.2. Photocatalytic test

2.2.1. Photocatalytic water oxidation to hydrogen peroxide

The reaction was performed in an open system by adding 4.0 mL of ion-exchanged water and the prepared CNPSP300 to a 5.9-mL quartz reactor irradiated with light using a 500 W xenon lamp. A HOYA UV-42 colored glass filter was used to control the wavelength of light. To compare the photoactivity of various polycyclic compounds, the powdered catalyst (3×10^{-5} mol) was added to ion-exchanged water and photo-irradiated under stirring. The potassium permanganate ($KMnO_4$) titration method was used to measure the amount of hydrogen peroxide produced [20].

2.2.2. Photocatalytic sterilization of Escherichia coli

E. coli (strain NBRC3301) was used for antibacterial activity experiments. Antibacterial activity was evaluated using the following procedure [21]. In a triangular flask, ion-exchanged water (300 mL), agar powder (4.5 g), and LB medium powder (6 g) were autoclaved at 121 °C for 20 min. After cooling for 2 h, the mixture was dispensed into plastic Petri dishes on a clean bench and allowed to cool until it solidified to form an LB solid medium. *E. coli* was scooped out with a platinum loop, inoculated into the solid medium using the fractional culture method,

and incubated at 37 °C overnight. A small amount of the obtained single colony of *E. coli* was scraped off with a platinum loop, inoculated into LB liquid medium, and incubated at 37 °C overnight while the medium was shaken from side to side with a shaker. The resulting *E. coli* solution was diluted 1000-fold with saline in an autoclaved container. In a 5.9-mL quartz tube reactor, 4 mL (10^5–10^6 CFU/mL) of the 1000-fold diluted *E. coli* solution and various catalysts (3×10^{-5} mol) were placed and exposed to visible-light or room light for 1 h. A 500 W xenon lamp was used for visible-light irradiation, and the wavelength of the light was controlled using a colored glass filter (HOYA UV-42). The light intensity was quantified as 40 W/m^2 using a light meter at 340 nm. Experiments under room light were performed by exposing the bacterial solution in the quartz reactor to the room light of a fluorescent lamp, without using a special light source. Using a light meter at 340 nm, the light intensity was determined as 0.1 W/m^2. The solution was further diluted 100-fold with saline, and 20 μL of this diluted solution was applied to the LB agar medium and incubated at 37 °C overnight. Colonies on the agar medium were counted after incubation; the numbers of viable cells before and after treatment were designated N_0 and N, respectively. The antibacterial rate was calculated from N and N_0 in the same manner as for yeast. The formula used was $(1 - N/N_0) \times 100$ (%).

2.2.3. Photocatalytic sterilization of yeast cells

Sugar (3.5 g) and agar powder (5.25 g) were added to beer (350 mL) and heated at 100 °C for 2 h to remove alcohol and carbonic acid from the liquid. Subsequently, the agar medium was dispensed into plastic Petri dishes and allowed to cool to room temperature until the medium solidified. Dry yeast powder was instead of bacteria. Dry yeast powder (0.01 g) was added to ion-exchanged water (100 mL) and stirred. The bacterial solution was diluted 10-fold with ion-exchanged water, and 10 μL was applied to the agar medium using a bacterial spreader. The Petri dish was then inverted and incubated at 37 °C for 50 h. The number of colonies that appeared on the agar medium was counted and designated N_0. As in the *E. coli* sterilization experiment, 4 mL of the dry yeast solution was placed in a quartz cylindrical reactor with the photocatalysts. The reactor was irradiated with a 500 W xenon lamp for 1 h. The wavelength of the light was controlled using a colored glass filter (HOYA UV-42). After light irradiation, the bacterial solution was diluted 10-fold with ion-exchanged water, and 10 μL of this diluted solution was applied to the agar medium and incubated in a Petri dish at 37 °C for 50 h. The number of colonies appearing on the agar medium was counted and designated N.

2.3. DFT calculation

Gaussian 09 software was used to calculate the most stable structures of the various polycyclic aromatic compounds. The HOMO and LUMO energy levels were obtained from the calculations. B3LYP methods using the 6–311 G (d, p) basis set were conducted using DFT calculations of all samples.

3. Results and discussion

3.1. Photocatalytic water oxidation to hydrogen peroxide over CNPSP300

Hydrogen peroxide was formed from water photooxidation using CNPSP300 as a photocatalyst, under visible-light irradiation. However, hydrogen peroxide was not produced when water was irradiated with visible-light in the absence of CNPSP300 and when a catalyst was added under dark conditions, indicating that water was photocatalytically oxidized over CNPSP300. Fig. 1 shows the time profile of the hydrogen peroxide yield when the water oxidation reaction was performed using the CNPSP300 photocatalyst. The hydrogen peroxide production rate is evidently high for up to 4 h of reaction time. However, the reaction rate decreases after 12 h, and hydrogen peroxide is scarcely produced from

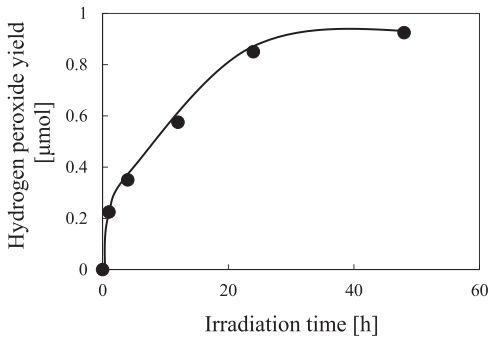

Fig. 1. Time profile of hydrogen peroxide yield for photocatalytic oxidation of water with CNPSP300 under visible-light irradiation.

24 to 48 h. This indicates that the reaction is terminated. Hydrogen peroxide decomposes by itself [22]. The decomposition and formation reactions of hydrogen peroxide are considered to occur simultaneously; with the increasing hydrogen peroxide concentration, the effect of hydrogen peroxide decomposition increases, the formation and decomposition rates attain equilibrium, and the reaction appears to stop. To examine the hydrogen peroxide degradation rate, 4.0 mL of an aqueous solution containing 1.8 μmol of hydrogen peroxide was prepared, and the time profile of hydrogen peroxide yield in the presence or absence of CNPSP300 was measured (Fig. 2). Hydrogen peroxide is degraded even under visible-light irradiation in the absence of a catalyst, and this degradation rate increases in the presence of the CNPSP300 photocatalyst under visible-light irradiation. The reduction potential of hydrogen peroxide is − 0.695 eV, which is higher than the LUMO potential (approximately −0.94 eV) of 5,8-dicyano[5]phenacene. Therefore, the excited electrons possibly reduce and decompose hydrogen peroxide. The hydrogen peroxide concentration does not increase at a certain concentration, presumably because the possibility of its decomposition by 5,8-dicyano[5]phenacene increases with increasing hydrogen peroxide concentration. Consequently, the formation and decomposition rates attain equilibrium.

Experiments were conducted to reuse CNPSP300 as a photocatalyst. The catalyst was collected after the reaction, washed with ion-exchanged water, and vacuum-dried overnight to obtain the reused catalyst. Table 1 lists the hydrogen peroxide yields obtained after 24 h of water oxidation. The yield for the second reused catalyst is approximately 80 % of the original. However, the hydrogen peroxide yields in the third and fourth reactions are approximately 90 % of the yields of the second and third reactions, respectively. This is presumably because 5,8-dicyano[5]phenacene was physically supported on the glass substrate via vacuum deposition, and the organic semiconductor was peeled off from the substrate in water, thereby decreasing the activity. However, the catalyst is not significantly damaged, suggesting the possibility of reuse.

Although the details of the hydrogen peroxide formation mechanism

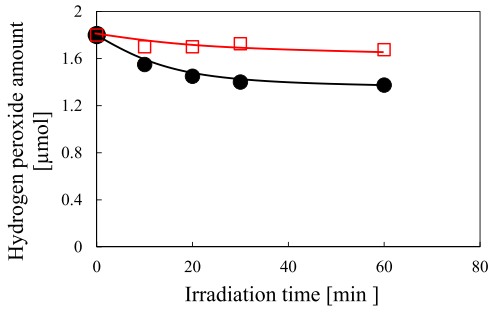

Fig. 2. Time profile of hydrogen peroxide amount for decomposition with CNPSP300 (●) and without the catalyst (□) under visible-light irradiation.

Table 1
Recycle tests of CNPSP300 photocatalyst for water oxidation under visible-light irradiation for 24 h[a].

Cycle number (-)	Hydrogen peroxide yield (μmol)
1	0.85
2	0.65
3	0.60
4	0.55

[a] For the reuse experiment, the catalyst was collected after the reaction, washed with ion-exchanged water, and vacuum-dried overnight at room temperature (25 °C).

in this reaction are unclear, the following is discussed [23–25].

Oxidation of water by produced holes.

$$H_2O + h^+ \rightarrow \bullet OH + H^+$$

$$2\ \bullet OH + 2\ h^+ \rightarrow O_2 + 2\ H^+$$

Reduction of oxygen by excited electrons.

$$O_2 + e^- \rightarrow \bullet O_2^-$$

$$\bullet O_2^- + H^+ \rightarrow HO_2\bullet$$

$$HO_2\bullet + H^+ + e^- \rightarrow H_2O_2$$

The produced holes (h^+) oxidize water to produce oxygen . In contrast, the excited electrons (e^-) reduce oxygen to produce hydrogen peroxide. In this process, superoxide anion radicals ($\bullet O_2^-$) and hydroxyl radicals (•OH) are formed as reaction intermediates. These superoxide anion radicals and hydroxyl radicals are characterized by strong oxidizing power and are therefore known to demonstrate antibacterial effects. The antibacterial effect of titanium dioxide photocatalysts is attributed to the formation of these oxygen species. In Section 3.2, we discuss the antibacterial effect of the CNPSP300 photocatalyst, which can produce hydroxyl radicals and superoxide anion radicals.

3.2. Photocatalytic sterilization of E. coli over CNPSP300

To evaluate the antibacterial performance of the CNPSP300 catalyst, its ability to sterilize *E. coli* under visible-light irradiation was tested. Fig. 3 shows the time profile of the inactivation rate of *E. coli* when CNPSP300 was introduced into the *E. coli* solution and irradiated with visible-light using a xenon lamp. Fig. 4 shows the time profile of the inactivation rate of *E. coli* under room light. When only light was irradiated without the photocatalyst, *E. coli* was inactivated over time under both the light irradiation conditions. For visible-light irradiation by xenon lamps, UV light is blocked by colored glass filters. However, despite using colored glass filters, approximately 10 % of UV light is known to leak in, and this UV light sterilizes *E. coli* bacteria even without photocatalysts. Fig. 3 shows that the CNPSP300 photocatalyst

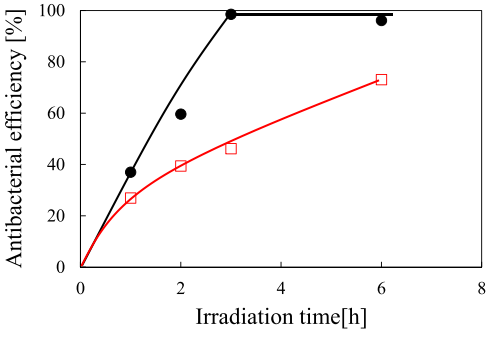

Fig. 3. Time profile of antibacterial efficiency against *E. coli* with CNPSP300 (•) or without catalyst (□) under visible-light irradiation.

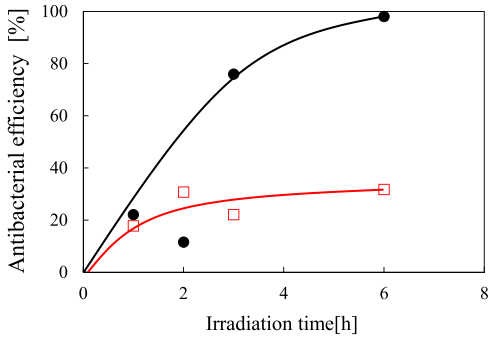

Fig. 4. Time profile of antibacterial efficiency against *E. coli* with CNPSP300 (•) or without catalyst (□) under room light irradiation.

introduced under visible-light irradiation significantly sterilizes *E. coli*. After approximately 3 h of visible-light irradiation, *E. coli* is completely sterilized. These results suggest that CNPSP300 exhibits antibacterial activity owing to its photocatalytic ability. Furthermore, the antibacterial effect of the CNPSP300 photocatalyst is more pronounced under room light, and *E. coli* is completely sterilized in approximately 6 h even at low light levels, suggesting that the CNPSP300 photocatalyst does not require a special light source such as xenon lamps, and natural light is sufficient and practical for its antibacterial effect on *E. coli*.

3.3. Photocatalytic test over the several powdered polycyclic aromatic compound derivatives

To evaluate other derivatives of polycyclic aromatic compounds that exhibit antibacterial activity, DFT calculations were used to identify catalysts that could generate hydrogen peroxide, and their actual hydrogen peroxide generation capacity and antibacterial effect were examined. Thin-film catalysts were not used for the reaction. Instead, powdered catalysts were used for comparing the activity. This is because differences such as the ease of fabricating thin-film catalysts are not apparent when compared to a suspension solution system. Table 2 lists the results of hydrogen peroxide production after visible-light irradiation for 24 h, and the antibacterial effect of each photocatalyst after visible-light irradiation for 1 h. Based on the data presented in Table 2, Fig. S5 depicts the correlation between the amount of hydrogen peroxide produced and the antibacterial efficiency of each photocatalyst, which is subjected to visible-light irradiation for 1 h. The amount of hydrogen peroxide produced and the antibacterial effect demonstrate a good relationship, although the plot is not linear only for 9,10-dicyanoanthracene, because the antibacterial efficiency reaches 100.00 % at an early stage. Scheme 1 shows the structural formulas of the polycyclic aromatic compound derivatives. The energy levels of water oxidation and oxygen reduction in the proposed hydrogen peroxide formation reaction are + 0.695 and + 1.23 eV, respectively [26]. Moreover, the HOMO and LUMO energy levels do not directly affect the hydrogen peroxide generation activity. However, the more efficiently the catalyst produces hydrogen peroxide, the higher its antibacterial effect. Anthracene derivatives produce more hydrogen peroxide, and their antibacterial effects are higher than those of other polycyclic aromatic compound derivatives. Anthracene is known to be highly unstable because the photodimerization reaction generally occurs at the 9- and 10-positions [27]. This reaction can be suppressed by introducing substituents at the positions where dimerization occurs. However, the catalyst with substituents only at the 9-position exhibit poor stability and cannot be reused. In contrast, 9,10-dicyanoanthracene with substituents at the 9- and 10-positions is extremely stable (Figs. S5–S7) and retains its activity in a recycling experiment involving yeast (Table 3).

These results indicate that a close relationship exists between the hydrogen peroxide production capacity and antibacterial activity and

Table 2
Results of catalytic water oxidation to hydrogen peroxide and antibacterial efficiency against *E. coli* in the presence of several polycyclic aromatic compound derivatives photocatalysts, and HOMO–LUMO energy levels and energy gaps of the catalysts (from DFT calculations).

Catalysts	Catalytic test		DFT calculation		
	H_2O_2 production (μmol)[a]	Antibacterial efficiency (%)[b]	HOMO (eV)	LUMO (eV)	Energy gap (eV)
2,7-dicyanopyrene	0.62	38.45	2.06	−0.84	2.90
5,8-dicyano[5]phenacene	0.88	37.34	1.86	−0.94	2.80
[5]phenacene-13-carboxylic acid	1.01	42.03	1.46	−1.54	3.00
9-cyanoanthracene	1.61	72.94	1.56	−0.84	2.40
9-nitroanthracene	1.82	79.10	1.56	−0.74	2.30
9,10-dicyanoanthracene	2.91	100.00	1.76	−0.34	2.10

[a] Water was irradiated by visible-light for 24 h at room temperature in the presence of oxygen.
[b] The *E. coli* solution was irradiated by visible-light for 1 h at room temperature.

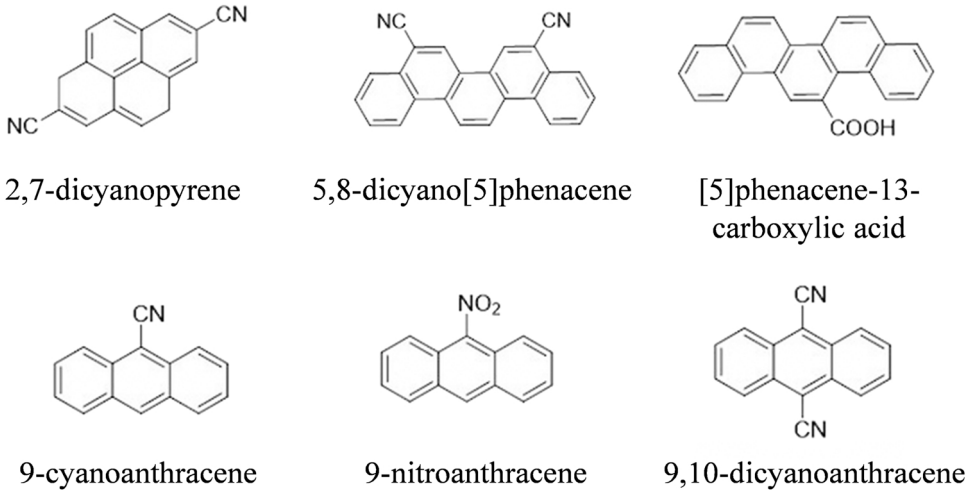

Scheme 1. Structural formulas of various polycyclic aromatic compound derivatives used in the reaction.

Table 3
Recycle tests of 9,10-dicyanoanthracene photocatalyst for yeast inactivation under visible-light irradiation for 1 h.

Cycle number (-)	Antibacterial efficiency (%)
1	100.00
2	99.80
3	99.80

that *E. coli* is possibly sterilized by oxygen species such as superoxide anion radicals and hydroxyl radicals, which are formed in the hydrogen peroxide production reaction.

3.4. Photocatalytic sterilization of E. coli over the powdered 9,10-dicyanoanthracene

The bactericidal effect of the 9,10-dicyanoanthracene powdered catalysts on *E. coli* was investigated in detail. Fig. 5 shows the time profile of the antibacterial efficiency of the 9,10-dicyanoanthracene powdered catalysts under visible-light irradiation. The antibacterial efficiency reaches 100 % at 20 min after the reaction is initiated. Assuming a first-order irreversible reaction with reference to the bacterial solution concentration, the rate constant for 5,8-dicyano[5]phenacene is 7.6×10^{-3} (min^{-1}), whereas the rate constant for 9,10-dicyanoanthracene is 0.12 (min^{-1}), indicating that 9,10 dicyanoanthracene is approximately 16 times faster than 5,8-dicyano[5]phenacene. For comparison, Table 4 presents the antibacterial efficiencies of 9,10-dicyanoanthracene, 5,8-dicyano[5]phenacene, and titanium dioxide powders after 1 h of reaction under room light. *E. coli* is sterilized even in non-catalytic reactions (Table 4). We assume that *E. coli* is

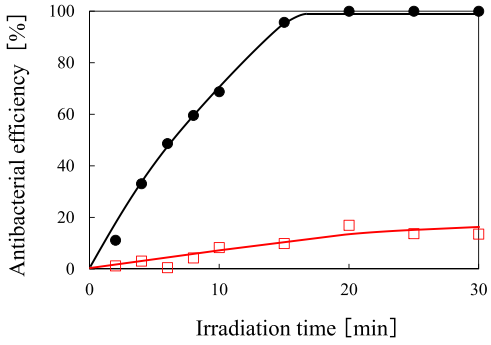

Fig. 5. Time profile of antibacterial efficiency against *E. coli* with 9,10-dicyanoanthracene (•) or without catalyst (□) under visible-light irradiation.

Table 4
Antibacterial efficiencies of various photocatalysts against *E. coli* under room light irradiation for 1 h.

Catalyst	Antibacterial efficiency (%)
none	8.33
5,8-dicyano[5]phenacene	22.67
9,10-dicyanoanthracene	45.40
Titanium oxide	30.83

sterilized by a small amount of UV light in the room light. When exposed to room light for 1 h, 9,10-dicyanoanthracene powdered catalyst exhibits an antibacterial efficiency of 45.40 %. However, the antibacterial efficiency is 22.67 % with the 5,8-dicyano[5]phenacene powdered

catalyst. Furthermore, the commonly used anatase-type titanium dioxide powdered catalyst has an antibacterial efficiency of 30.83 %, indicating that the antibacterial performance of the 9,10-dicyanoanthracene powdered catalyst is excellent. Thus, 9,10-dicyanoanthracene is a highly effective photocatalyst with antibacterial activity.

3.5. Estimation of oxygen species responsible for antibacterial activity

The antibacterial action may be caused directly by the generated hydrogen peroxide rather than by oxygen species such as superoxide anion radicals ($\bullet O_2^-$) and hydroxyl radicals ($\bullet$OH), which are reaction intermediates that are generated in the field. Therefore, antibacterial activity was investigated by irradiating the bacterial solution with visible-light in a system where only hydrogen peroxide was added. The antibacterial activity was approximately the same as that of the control, indicating that the hydrogen peroxide produced was not directly responsible for the antibacterial activity (Table S1). Based on the results presented in Fig. S5, we hypothesized that a relationship exists between the amount of hydrogen peroxide produced and the antibacterial effect, and that the radical species formed during the hydrogen peroxide production cause the antibacterial effect.

To identify the oxygen species that mainly exert antibacterial activity, a trapping reagent that scavenges superoxide anion radicals and hydroxyl radicals species was added to the bacterial solution, irradiated with visible-light for 0.5 h, and its behavior was examined. Specifically, 4-hydroxy-2,2,6,6-tetramethylpiperidine-1-oxyl (TEMPOL) was added as a reagent to trap superoxide anion radicals and isopropyl alcohol (IPA) to trap hydroxyl radicals [23]. The above trapping reagents were added individually without a catalyst and irradiated with visible-light for 1 h. However, the antibacterial efficiencies were similar to that of the control, suggesting that the trapping reagents alone had no bactericidal action. Fig. 6 shows the results when 0.29 μmol of 9,10-dicyanoanthracene powder catalyst and TEMPOL or IPA were added to the bacterial solution and irradiated with visible-light for 1 h. When only 9,10-dicyanoanthracene was added to the bacterial solution, the antibacterial efficiency was 100.00 %. However, when TEMPOL was added and visible-light was irradiated, the antibacterial efficiency decreased to 62.23 %. When IPA was added and visible-light was irradiated, the antibacterial efficiency was further decreased to 21.46 %, indicating that IPA affected the antibacterial efficiency to a greater extent than TEMPOL. This suggests that both superoxide anion radicals and hydroxyl radicals produce antibacterial effects; however, the formation of hydroxyl radicals is particularly significant, although both oxygen species are responsible for the antibacterial effect. Subsequently, 5,8-dicyano[5]phenacene and 9,10-dicyanoanthracene photocatalysts were irradiated with visible-light in the presence of oxygen, and 5,5-dimethyl-1-pyrroline N-oxide (DMPO) was used as a spin-trapping regent for superoxide anion radicals. The electron spin resonance spectra for 5,8-dicyano[5]phenacene and 9,10-dicyanoanthracene are shown in Figs. S9 and S10, respectively. No spectrum is observed in the absence of visible-light irradiation. However, after 10 min of visible-light irradiation, a peak attributed to DMPO-$\bullet O_2^-$ is observed for both photocatalysts, indicating that superoxide anion radicals are formed when the photocatalysts are subjected to visible-light irradiation in the presence of oxygen. After 20 min of visible-light irradiation, the intensities of 5,8-dicyano[5]phenacene and 9,10-dicyanoanthracene photocatalysts increase by approximately 1.6 and 1.4 times, respectively, compared with the intensities after 10 min of irradiation. We speculate that a correlation exists between the amount of radical species formed and the antibacterial activity.

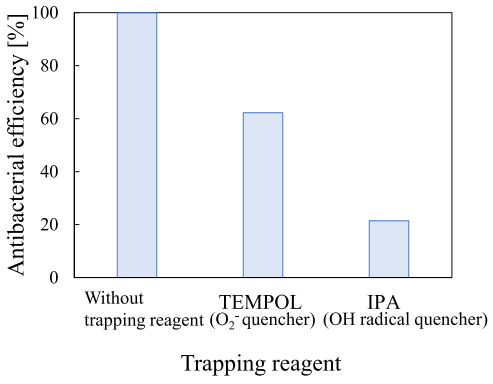

Fig. 6. Antibacterial efficiency of 9,10-dicyanoanthracene with or without trapping reagents against *E. coli* under visible-light irradiation for 0.5 h.

4. Conclusions

The CNPSP300 thin-film catalyst, in which 5,8-dicyano[5]phenacene was supported on a silica plate via vacuum deposition, was found to function as a photocatalyst under visible-light irradiation, producing hydrogen peroxide by the photooxidation of water with oxygen. In this process, oxygen species, such as superoxide anion radicals and hydroxyl radicals, are generated as reaction intermediates. Because these species are known to cause photocatalytic antibacterial effects, we investigated the antibacterial effects of the CNPSP300 thin-film photocatalyst under visible-light irradiation. Antibacterial experiments using *E. coli* on a CNPSP300 thin-film photocatalyst showed that CNPSP300 can sterilize *E. coli* under visible-light irradiation. The antibacterial performance of the catalyst under room light also suggests that it is considerably practical. Using DFT calculations, we found that several polycyclic aromatic compound derivatives could produce hydrogen peroxide from water oxidation under visible-light irradiation, and the reaction proceeded when these catalysts were used. In particular, 9,10-dicyanoanthracene is highly stable and produces a substantial amount of hydrogen peroxide via water oxidation; moreover, its antibacterial activity under visible-light irradiation is approximately 16 times that of 5,8-dicyano[5]phenacene, which is also an excellent photocatalyst. The oxygen species responsible for these antibacterial effects were examined using trapping reagents, revealing that both superoxide anion radicals and hydroxyl radicals cause these antibacterial effects, with hydroxyl radicals being particularly effective. These polycyclic aromatic compound derivatives can be prepared as thin-films via vacuum evaporation, sputtering, or spraying and can also be supported by chemical bonding, making them extremely convenient and practical for applications in the future.

Funding

This work was supported by JSPS KAKENHI (grant number 22K04827).

CRediT authorship contribution statement

Yuichi Ichihashi: Supervision, Conceptualization, Project administration, Funding acquisition, Methodology, Writing – original draft. **Tomoya Sekiguchi:** Investigation, Writing – original draft. **Koki Hiramatsu:** Investigation, Visualization, Writing – original draft. **Yuya Tokui:** Methodology, Investigation, Visualization. **Kazuo Kumagai:** Investigation, Resources.' **Hideto Matsuyama:** Methodology, Resources. **Keita Taniya:** Methodology, Writing – review & editing. **Satoru Nishiyama:** Methodology, Writing – review & editing.

Declaration of Competing Interest

The authors declare that they have no known competing financial interests or personal relationships that could have appeared to influence the work reported in this paper.

Data Availability

The data that has been used is confidential.

Acknowledgments

The authors would like to express their deepest gratitude to Professor Hiroshi Danjo of Konan University for his advice on the synthesis of polycyclic aromatic compound derivatives. The authors would like to thank Editage (www.editage.com) for English language editing.

Appendix A. Supporting information

Supplementary data associated with this article can be found in the online version at doi:10.1016/j.apcatb.2022.122326.

References

[1] M.D. Arienzo, J. Carbajo, A. Bahamonde, M. Crippa, S. Polizzi, R. Scotti, L. Wahba, F. Morazzoni, Photogenerated defects in shape-controlled TiO_2 anatase nanocrystals: A probe to evaluate the role of crystal facets in photocatalytic processes, J. Am. Chem. Soc. 133 (2011) 17652–17661, https://doi.org/10.1021/ja204838s.

[2] A. Okemoto, K. Tanaka, Y. Kudo, S. Gohda, Y. Koshiba, K. Ishida, T. Horie, K. Taniya, Y. Ichihashi, S. Nishiyama, Hydrogen production for photocatalytic decomposition of water with urea as a reducing agent, Catal. Today 307 (2018) 231–236, https://doi.org/10.1016/j.cattod.2017.01.035.

[3] U.I. Gaya, A.H. Abdullah, Heterogeneous photocatalytic degradation of organic contaminants over titanium dioxide: a review of fundamentals, progress and problems, Author links open overlay panel, J. Photochem. Photobiol. C. 9 (2008) 1–12, https://doi.org/10.1016/j.jphotochemrev.2007.12.003.

[4] K. Obata, K. Kishishita, A. Okemoto, K. Taniya, Y. Ichihashi, S. Nishiyama, Photocatalytic decomposition of NH_3 over TiO_2 catalysts doped with Fe, Appl. Catal. B 160–161 (2014) 200–203, https://doi.org/10.1016/j.apcatb.2014.05.033.

[5] U. Baig, M.A. Ansari, M.A. Gondal, S. Akhtar, F.A. Khan, W.S. Falath, Single step production of high-purity copper oxide-titanium dioxide nanocomposites and their effective antibacterial and anti-biofilm activity against drug-resistant bacteria, Mater. Sci. Eng. C. 113 (2020), 110992, https://doi.org/10.1016/j.msec.2020.110992.

[6] B. Kim, D. Kim, D. Cho, S. Cho, Bactericidal effect of TiO_2 photocatalyst on selected food-borne pathogenic bacteria, Chemosphere 52 (2003) 277–281, https://doi.org/10.1016/S0045-6535(03)00051-1.

[7] D.H. Song, S.H. Uhm, S.E. Kim, J.S. Kwon, J.G. Han, K.N. Kim, Synthesis of titanium oxide thin films containing antibacterial silver nanoparticles by a reactive magnetron co-sputtering system for application in biomedical implants, Mater. Res. Bull. 47 (2012) 2994–2998, https://doi.org/10.1016/j.materresbull.2012.04.085.

[8] M.N. Chong, B. Jin, C.W.K. Chow, C. Saint, Recent developments in photocatalytic water treatment technology: A review, Water Res. 44 (2010) 2997–3027, https://doi.org/10.1016/j.watres.2010.02.039.

[9] H.T. Nguyen, H.M. Bui, Y.F. Wang, S.J. You, Antifouling CuO@TiO_2 coating on plasma-grafted PAA/PES membrane based on photocatalysis and hydrogen peroxide activation, *Environ. Sci. Pollut. Res.*, *in press.* ⟨https://doi.org/10.1007/s11356–022-23005–9⟩.

[10] S. Dong, L. Cui, W. Zhang, L. Xia, S. Zhou, C.K. Russell, M. Fan, J. Feng, J. Sun, Double-shelled $ZnSnO_3$ hollow cubes for efficient photocatalytic degradation of antibiotic wastewater, Chem. Eng. J. 384 (2020), 123279, https://doi.org/10.1016/j.cej.2019.123279.

[11] D. Lu, G. Zhang, Z. Wan, Visible-light-driven g-C_3N_4/Ti^{3+}-TiO_2 photocatalyst co-exposed {0 0 1} and {1 0 1} facets and its enhanced photocatalytic activities for organic pollutant degradation and Cr(VI) reduction, Appl. Surf. Sci. 358 (2015) 223–230, https://doi.org/10.1016/j.apsusc.2015.08.240.

[12] S. Naserian, M. Izadyar, E. Ranjbakhsh, Theoretical evaluation of charge transport properties and mobility of tetraphenyldipyranylidene derivatives in organic field-effect transistors, J. Photochem. Photobio. A 435 (2023), 114283, https://doi.org/10.1016/j.jphotochem.2022.114283.

[13] G. Gelinck, P. Heremans, K. Nomoto, T.D. Anthopoulos, Organic transistors in optical displays and microelectronic applications, Adv. Mater. 22 (2010) 3778–3798, https://doi.org/10.1002/adma.200903559.

[14] A.F. Paterson, S. Singh, K.J. Fallon, T. Hodsden, Y. Han, B.C. Schroeder, H. Bronstein, M. Heeney, I. McCulloch, T.D. Anthopoulos, Recent progress in high-mobility organic transistors: a reality check, Adv. Mater. 30 (2018) 1801079, https://doi.org/10.1002/adma.201801079.

[15] J.T. Kintigh, J.L. Hodgson, A. Singh, C. Pramanik, A.M. Larson, L. Zhou, J.B. Briggs, B.C. Noll, E. Kheirkhahi, K. Pohl, N.E. McGruer, G.P. Miller, A Robust, high-temperature organic semiconductor, J. Phys. Chem. C. 118 (2014) 26955–26963, https://doi.org/10.1021/jp505011x.

[16] H. Sun, A. Putta, M. Billion, Arene, Trifluoromethylation: An effective strategy to obtain air-stable n-type organic semiconductors with tunable optoelectronic and electron transfer properties, J. Phys. Chem. A 116 (2012) 8015–8022, https://doi.org/10.1021/jp301718j.

[17] A. Okemoto, K. Kishishita, S. Maeda, S. Gohda, M. Misaki, Y. Koshiba, K. Ishida, T. Horie, K. Taniya, Y. Ichihashi, S. Nishiyama, Application of picene thin-film semiconductor as a photocatalyst for photocatalytic hydrogen formation from water, Appl. Catal. B 192 (2016) 88–92, https://doi.org/10.1016/j.apcatb.2016.03.028.

[18] Y. Ichihashi, T. Sekiguchi, Y. Tokui, R. Hori, S. Naito, Y. Koshiba, Y. Sutani, K. Ishida, K. Taniya, S. Nishiyama, Decomposition of water over picene derivatives photocatalyst under visible light irradiation, Catal. Today 410 (2023) 317–322. ⟨https://doi.org/10.1016/j.cattod.2022.06.008⟩.

[19] T. Shanmuganathan, A.A.M. Prince, N. Dhatchanamoorthy, K. Parthasarathy, M. Venugopal, Synthesis anti-inflammatory activity of picen-13ylmethylene derivatives, ARKIVOC part v (2017) 67–69, https://doi.org/10.24820/ark.5550190.p010.100.

[20] N.V. Klassen, D. Marchington, H.C.E. McGowan, H_2O_2 determination by the I_3^- method and by $KMnO_4$ titration, Anal. Chem. 66 (1994) 2921–2925, https://doi.org/10.1021/ac00090a020.

[21] M.F. Dadjour, C. Ogino, S. Matsumura, S. Nakamura, N. Shimizu, Disinfection of Legionella pneumophila by ultrasonic treatment with TiO_2, Water Res. 40 (2006) 1137–1142, https://doi.org/10.1016/j.watres.2005.12.047.

[22] K. Iwamatsu, S. Sundin, J.A. LaVerne, Hydrogen peroxide kinetics in water radiolysis, Radiat. Phys. Chem. 145 (2018) 207–212, https://doi.org/10.1016/j.radphyschem.2017.11.002.

[23] Y. Yang, G. Zeng, D. Huang, C. Zhang, D. He, Ch Zhou, W. Wang, W. Xiong, X. Li, B. Li, W. Dong, Y. Zhou, Molecular engineering of polymeric carbon nitride for highly efficient photocatalytic oxytetracycline degradation and H_2O_2 production, Appl. Catal. B 272 (2020), 118970, https://doi.org/10.1016/j.apcatb.2020.118970.

[24] Y. Shiraishi, T. Takii, T. Hagi, S. Mori, Y. Kofuji, Y. Kitagawa, S. Tanaka, S. Ichikawa, T. Hirai, Resorcinol–formaldehyde resins as metal-free semiconductor photocatalysts for solar-tohydrogen peroxide energy conversion, Nat. Mater. 18 (2019) 985–993, https://doi.org/10.1038/s41563-019-0398-0.

[25] S. Dong, L. Cui, W. Zhang, L. Xia, S. Zhou, C.K. Russell, M. Fan, J. Feng, J. Sun, Double-shelled ZnSnO3 hollow cubes for efficient photocatalytic degradation of antibiotic wastewater, Chem. Eng. J. 384 (2020), 123279, https://doi.org/10.1016/j.cej.2019.123279.

[26] X. Zeng, Y. Liu, Y. Kang, Q. Li, Y. Xia, Y. Zhu, H. Hou, M.H. Uddin, T. R. Gengenbach, D. Xia, C. Sun, D.T. Mccarthy, A. Deletic, J. Yu, X. Zhang, Simultaneously tuning charge separation and oxygen reduction pathway on graphitic carbon nitride by polyethylenimine for boosted photocatalytic hydrogen peroxide production, ACS Catal. 10 (2020) 3697–3706, https://doi.org/10.1021/acscatal.9b05247.

[27] H. Bouas-Laurent, A. Castellan, J.P. Desvergne, R. Lapouyade, Photodimerization of anthracenes in fluid solution: structural aspects, Chem. Soc. Rev. 29 (2000) 43–55, https://doi.org/10.1039/A801821I.